Hindawi Publishing Corporation
Journal of Nanomaterials
Volume 2015, Article ID 167569, 7 pages
http://dx.doi.org/10.1155/2015/167569

Research Article

Impact of NiO_x Buffer Layers on the Dielectric Properties of $BaTiO_3$ Thin Films on Nickel Substrates Fabricated by Polymer Assisted Deposition

Hui Du,[1] Yang Li,[1] Wei Zheng Liang,[1] Yu Xuan Wang,[1] Min Gao,[1] Wen Huang,[1] Yin Zhang,[1] and Yuan Lin[1,2]

[1]*State Key Laboratory of Electronic Thin Films and Integrated Devices, University of Electronic Science and Technology of China, Chengdu, Sichuan 610054, China*
[2]*Institute of Electronic and Information Engineering in Dongguan, University of Electronic Science and Technology of China, Dongguan, Guangdong 523808, China*

Correspondence should be addressed to Yuan Lin; linyuan@uestc.edu.cn

Received 26 January 2015; Revised 23 May 2015; Accepted 28 May 2015

Academic Editor: Joydeep Dutta

Structural health monitoring with piezoelectric thin films integrated on structural metals shows great advantages for potential applications. However, the integration of piezoelectric thin films on structure metals is still challenged. In this paper, we report the piezoelectric barium titanate [$BaTiO_3$ (BTO)] thin films deposited on polycrystalline Ni substrates by the polymer assisted deposition (PAD) method using NiO_x as the buffer layers. The NiO_x buffer layers with different thicknesses were prepared by varying immersing time from 5 minutes to 4 hours in H_2O_2 solution. The dielectric and leakage current properties of the thin films have been studied by general test systems. The BTO/Ni heterostructure with 2-hour immersing time exhibits better dielectric properties with a dielectric constant over 1500 and a 34.8% decrease of the dielectric loss compared to that with 5-minute immersing time. The results show that the leakage current density is strongly affected by the thickness of the NiO_x buffer layer. The conduction mechanisms of the BTO/Ni heterostructure have been discussed according to the J-V characteristic curves.

1. Introduction

Nanomaterials, including nanodots, nanowires, nanothin films, and related composites, have been immensely investigated in the last few decades due to their wide potential applications [1–5]. Barium titanate [$BaTiO_3$ (BTO)] thin film, noted for its high dielectric constant and ferroelectric and piezoelectric properties, has aroused much attention for its potential applications in dynamic random access memories, optical modulators, waveguides, structural health monitoring (SHM), and microelectromechanical system (MEMS) [6–8]. With the increasing demands on embedded high density capacitors in the microelectronic packages and piezoelectric-based SHM, investigation on the fabrication of BTO thin films on base metallic substrates such as Ni or Cu has been initiated. Particularly, piezoelectric-thin-film-based built-in active SHM sensors with nondestructive evaluation abilities have shown great advantages compared to the bulk ones due to their seamless atomic bond between the active sensor and the structure as well as their low voltage requirement [9]. However, major challenges exist in the fabrication of piezoelectric thin films on structural materials due to the difficulties in controlling the oxidation of the structural metallic substrates, the interdiffusion, and the crystallization of the oxide piezoelectric thin films. The growth of BTO thin films on noble metals such as Pt and Au coated Si substrates or metal-oxide substrates has been widely reported by using the techniques of pulsed laser deposition (PLD), sputtering, or chemical solution deposition (CSD) [10–13]. Nevertheless, only a few groups have initiated the efforts of how to fabricate BTO thin films on nickel foils using CSD and PLD methods [14–17].

In 2004, a chemical solution deposition technique named polymer assisted deposition (PAD) [18–20] was reported,

which has proved itself as a promising complementary film fabrication technique with the advantages of low cost, precursor solution stability, and process controllability [21]. We have demonstrated that BTO films could be directly deposited on nickel substrates by using the PAD technique [22–24]. Specifically, NiO_x layer must be formed on the Ni substrate by pretreating it in H_2O_2 solution prior to the thin film deposition and the precursor wet films must be thermally treated in a reduced environment. On one hand, NiO_x layer serves as a buffer layer to improve the wettability of the substrates and prevent interdiffusion at the interface during annealing. On the other hand, the free energy of BTO (−1854 kJ/mol, at 1100 K) is much lower than that of NiO (−315 kJ/mol, at 1100 K) [25], and BTO has the ability to deprive oxygen from NiO_x layer. In other words, NiO_x buffer layer also serves as the oxygen source during the annealing process of the BTO films in a reduced environment, which would to some degree release the concern of oxygen vacancies in the as-prepared BTO films. Reasonable dielectric constant and dielectric loss can be achieved for the optimized as-prepared BTO thin films. Decreased leakage current densities have been observed in the films with the pretreated NiO_x layers compared to the reference sample. To get a deep understanding on the effect of NiO_x layer, a systematic study on the leakage mechanism in this specific structure is necessary.

2. Materials and Methods

Details for the preparation of BTO film on nickel substrate by PAD method have been reported in our previous work [22–24]. Firstly, nickel substrates whose thickness is 0.5 mm were polished to get a smooth and shiny surface. However, this kind of surface has a very poor wettability to the water-based precursor solutions used in PAD. Thus we immersed the nickel substrate into 10% hydrogen peroxide solution at 50°C, and the nickel on the surface was oxidized gradually. An oxide buffer layer NiO/Ni_2O_3 was formed to improve its wettability. In this experiment, by varying the immersing time of the Ni substrates in the H_2O_2 solution, different thicknesses of NiO_x buffer layers could be formed. We selected five different samples, and their immersing time in the H_2O_2 solution was 5 min (as the reference sample), 30 min, 1 h, 2 h, and 4 h, respectively.

The precursor solutions containing Ba^{2+} and Ti^{4+} were prepared according to the literature reports [18, 19]. Technically, Ba^{2+} solution was made by adding barium nitrate to the water solution of ethylenediaminetetraacetic acid (EDTA) and polyethyleneimine (PEI, from Sigma-Aldrich, average Mn≈60,000, Mw≈750,000). The solution was then purified and concentrated in an Amicon filtration unit to yield a solution with Ba^{2+} ions. To prepare the Ti^{4+} solution, titanium chloride was slowly added to 30% peroxide solution, then the solution was added slowly to the mixture of EDTA and PEI solution, and finally the solution was purified and concentrated to get a solution containing Ti^{4+} ions. The concentrations of Ba^{2+} and Ti^{4+} in the solutions were 19.8 and 12.4 mg/mL, respectively, measured by Inductively Coupled Plasma Optical Emission Spectrometer (ICP-OES). Figure 1(a) shows the pictures of the Ba^{2+} and Ti^{4+} solutions. The Ba^{2+} and Ti^{4+} solutions were then mixed in the molar ratio of 1 : 1 to yield a homogenous precursor solution for BTO.

The as-prepared solution was spin-coated on the pretreated nickel substrates with a spin rate of 3000 rpm for 30 seconds. The as-prepared samples were put into a furnace for heat treatment. The spin coating and thermal treatment process were repeated for 5 times. We treated the first layer of BTO thin films at 800°C to get distinct interface and the other layers at 600°C to avoid excessive thermal exposure of the nickel substrates. Then, the BTO thin films were annealed at 800°C in order to get fine crystallization. To avoid the oxidation of the Ni substrates, the whole thermal treatment process was performed in the flowing forming gas of 96% N_2 and 4% H_2 with a flow rate of 100 mL/min. After SEM detection, the final thickness of the BTO thin films is about 400 nm. Figure 1(b) schematically shows the heat treatment process.

The crystallinity of the films was first examined by the X-ray diffraction (XRD) technique. To measure the dielectric properties of the BTO thin films, Au electrodes with an area of 20 μm × 20 μm were deposited on the surfaces of BTO thin films by lithography and magnetron sputtering methods as the top electrodes. Dielectric properties of the samples were tested using an Agilent-4294A Precision LCR meter. Leakage currents were measured using an Agilent B2901A Precision Source/Measure Unit. Figure 2 shows the test sketch of BTO/Ni samples and dielectric property and leakage current test system. The applied voltage varied from −10 V to 0 V and then from 0 V to +10 V for the leakage current measurements.

3. Results and Discussion

XRD was performed using Cu K radiation to examine crystal structure of the BTO/Ni heterostructures. It is interesting to see that all the samples exhibit similar diffraction patterns. Typical results are shown in Figure 3 (only two samples with immersing time of 5 min and 4 h are shown here).

The characteristic peaks of polycrystalline nickel and pseudocubic BTO can be identified from the XRD pattern. Characteristic peaks of NiO and Ni_2O_3 cannot be observed despite different immersing time of nickel substrates in H_2O_2 solution (which refers to the oxidation time of nickel substrate). The results of XRD demonstrate that the BTO thin films have been successfully fabricated on polycrystalline nickel substrates without detectable nickel oxide phases.

Figures 4 and 5 show the dielectric constant and loss of these BTO/Ni heterostructures treated in H_2O_2 solution with different immersing time. The measurements were executed at 100 kHz and room temperature. From these two figures, the dielectric constant and the dielectric loss with immersing time of 5 min, 30 min, 1 h, 2 h, and 4 h are, respectively, 1722, 1657, 1600, 1581, and 253 and 2.3%, 2.2%, 1.9%, 1.5%, and 0.3%. Both dielectric constant and dielectric loss reduce with the increase of immersing time. This is mainly because of

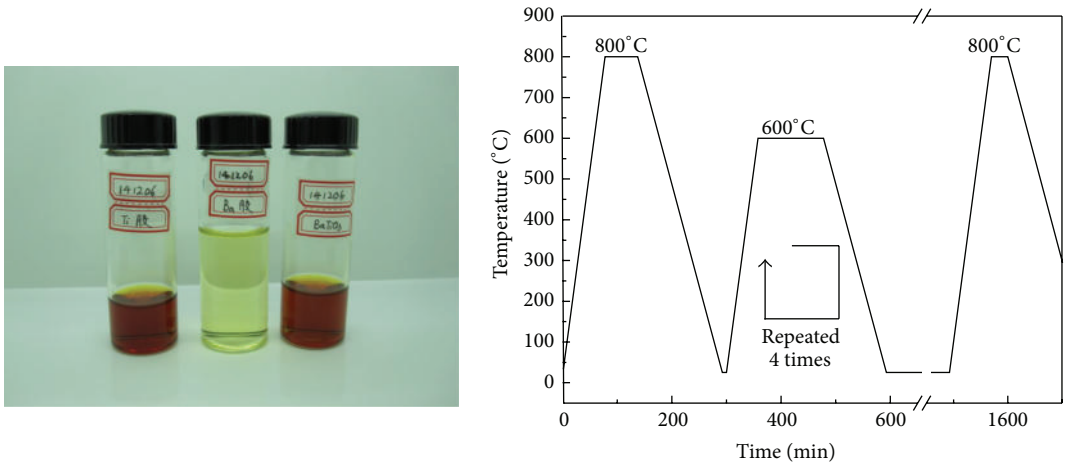

(a) (b)

Figure 1: (a) Pictures of Ba^{2+} solution and Ti^{4+} solution. (b) Schematic of heat treatment process of BTO/Ni samples.

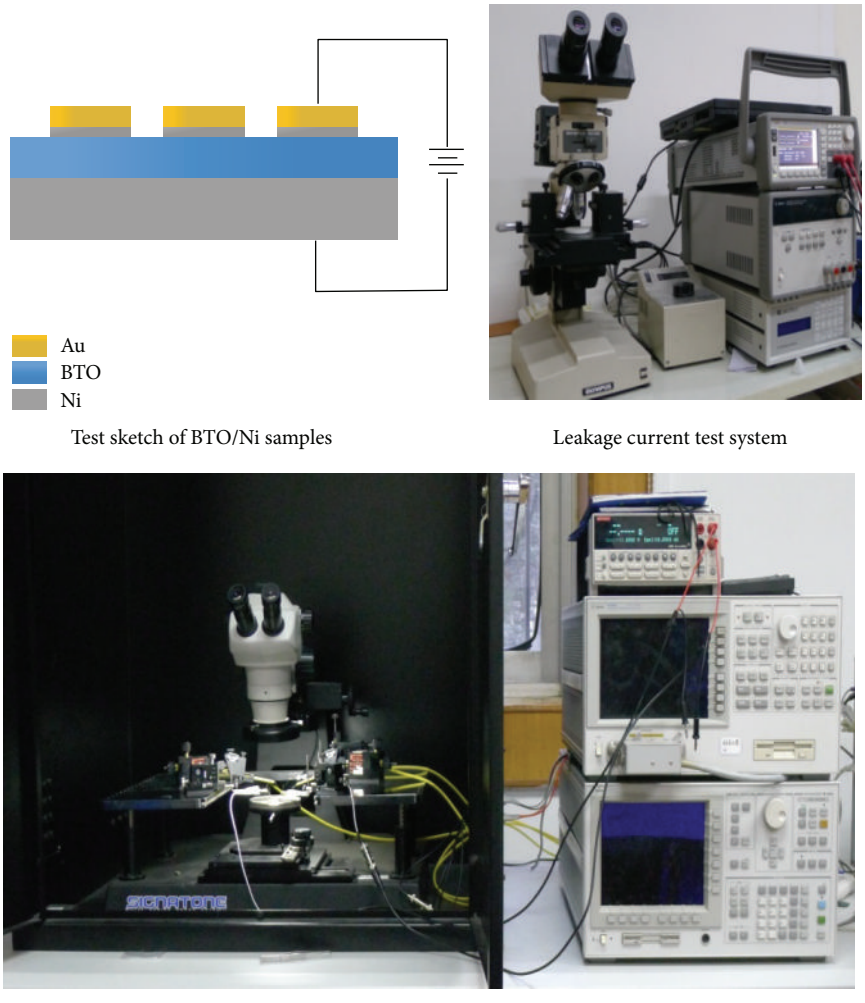

Test sketch of BTO/Ni samples

Leakage current test system

Dielectric property test system

Figure 2: The test sketch of BTO/Ni samples and dielectric property and leakage current test system.

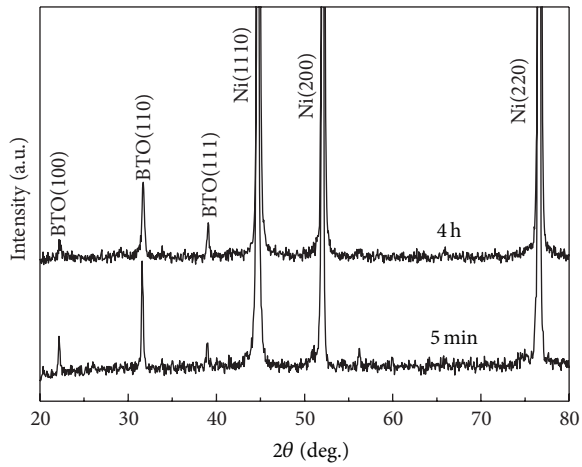

FIGURE 3: XRD patterns from θ-2θ scans of BTO/Ni samples.

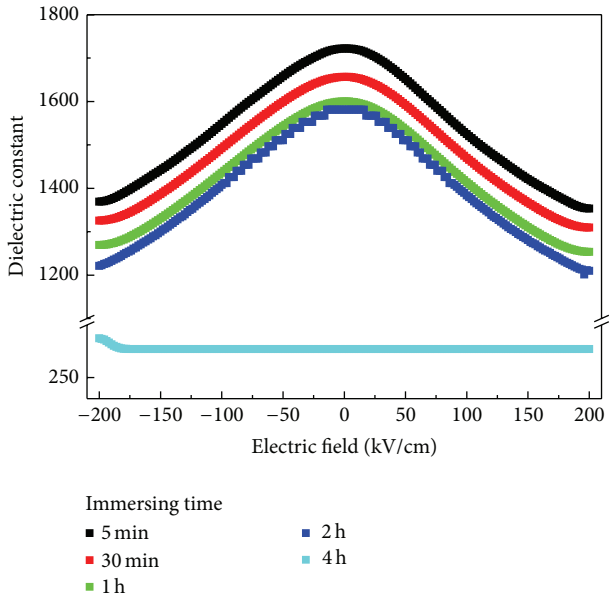

FIGURE 4: The dielectric constant characteristic curves of the BTO/Ni samples.

the influence of the nickel oxide buffer layers between the BTO thin films and the Ni substrates. The nickel oxide layer could block the interface diffusion between the Ni and the BTO layer and thus improve the quality of the BTO thin films and reduce the leakage current and dielectric loss. However, NiO_x layer has a much lower dielectric constant compared to the BTO layer, which implies that the heterostructure is actually a big capacitor of BTO in series with a small capacitor of NiO_x. Thus, the as-measured dielectric constant should be lower when NiO_x layer is thicker.

As can be seen from Figures 4 and 5, the balance should be considered when looking for the optimal pretreatment condition for the Ni substrates. For example, though the dielectric loss of the sample with 4 h immersing time decreases by 87% compared to the one with 5 min immersing time, the dielectric constant decreases by 85.3%. On the other hand,

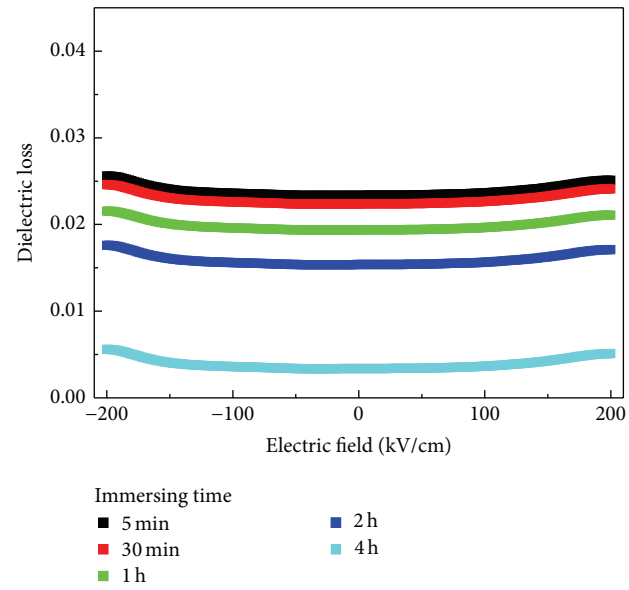

FIGURE 5: The dielectric loss characteristic curves of the BTO/Ni samples.

the dielectric constant of the sample with 2 h immersing time decreases only by 8.2%, whereas its dielectric loss reduced by 34.8% compared to the sample with 5 min immersing time. Therefore, 2 h immersing time might be an optimized condition for the applications which require low dielectric loss and high dielectric constant.

The Au electrode and the Ni substrate were regarded as positive and negative electrodes, respectively. In order to prevent the breakdown and obtain accurate leakage characteristic curve, the limit current and test delay time were set as 100 μA and 0.1 s, respectively. All the scanning sequences began with 0 V. The leakage current density and electric field characteristic curves for the samples with different immersing time are shown in Figure 6.

From Figure 6, we can see that the J-E characteristic curves are asymmetric under positive and negative bias voltage, which is mainly caused by the asymmetry of this kind of integrated structure. The leakage current conduction mechanism is then different when metal electrode is under positive and negative bias voltage. So it is necessary for us to analyze the leakage current conduction mechanism under positive and negative bias voltage, respectively. Whatever negative or positive bias voltage, leakage current decreases gradually along with the increase of immersing time. The sample with 4 h immersing time has a much lower leakage current density than the other 4 samples. This is mainly due to the increase of bulk resistance. As the oxidation time of nickel substrates increases, thickness of the nickel oxide layers increases. Since the films were thermally treated in a reduced ambient with the oxygen pressure of about 10^{-18} atm, nickel oxide will decompose gradually during the heat treatment process [26, 27]. And as mentioned ahead, since the free energy of BTO is much lower than that of NiO, the oxygen from NiO would diffuse into the BTO layer to compensate oxygen vacancies. It is believed that the oxygen vacancies

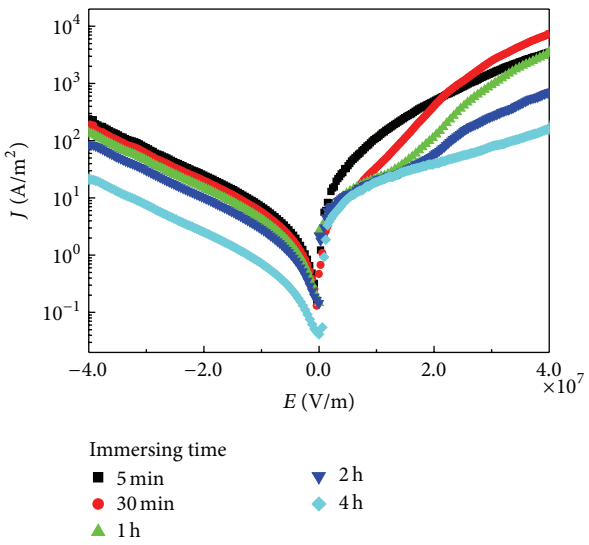

FIGURE 6: J-E characteristic curves under positive and negative biases.

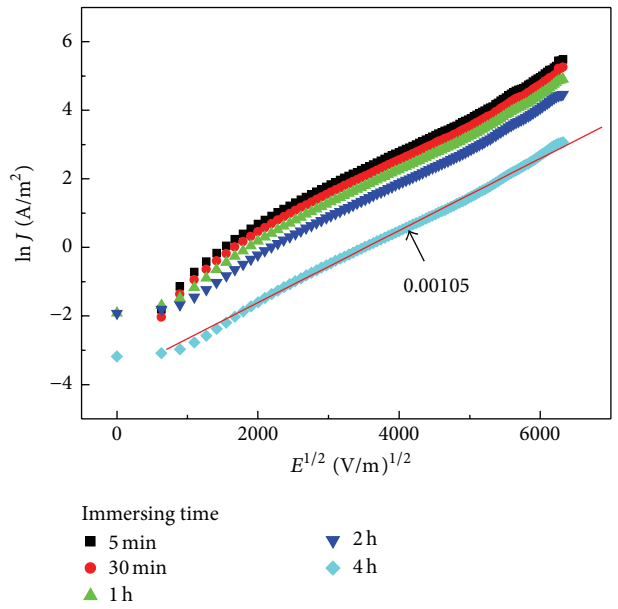

FIGURE 7: ln(J) versus $E^{1/2}$ plots under negative bias for the BTO/Ni samples.

are the key factor contributing to the leakage current in ferroelectric oxide thin films. Thus, the sample with a thicker NiO_x layer should have a lower leakage current density.

The leakage current conduction mechanism under negative bias is analyzed by plotting ln(J) versus $E^{1/2}$, as shown in Figure 7. It shows that all the curves fit well with the Schottky emission mechanism [28, 29], which can be expressed as

$$J = A^* T^2 \exp\left[\frac{-e\left(\phi_o - \sqrt{eE/4\pi\varepsilon_i\varepsilon_0}\right)}{kT}\right], \quad (1)$$

where J is the current density, A^* is the Richardson constant, T is the absolute temperature, e is elementary charge, E is the applied electric field, ε_i is the optical dielectric constant, ε_0 is the permittivity of free space, k is the Boltzmann constant, and $e\phi_0$ is the Schottky barrier height.

The optical dielectric constant of the BTO samples is about 1.95, as calculated from the slopes of the curves in Figure 7. The value is at the same order of magnitude but smaller than the reported optical dielectric constant of about 5 for BTO bulk [30]. The reason may come from the different quality of our BTO thin film samples with the reported bulks. The absolute values of the intercept of the curves in Figure 6 reflect the Schottky barrier height. It is interesting to see that the Schottky barrier height increases with the thickness of NiO_x layer. The reason may lie in the suppression of interdiffusion between the BTO layer and the Ni substrate when the thickness of NiO_x layer increases, which would increase the Schottky barrier height.

From Figure 8, it is seen that, under the positive voltage, all the curves basely conform to a transition from the Ohmic conductive mechanism to the space-charge-limited-current (SCLC) mechanism [31].

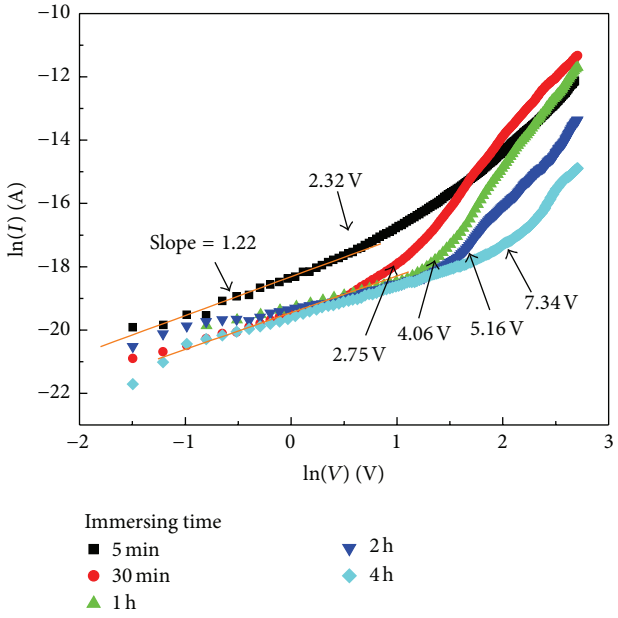

FIGURE 8: ln(I) versus ln(V) plots under positive bias for the BTO/Ni samples.

For the Ohmic conductive mechanism, the current density and the applied electric field follow a linear relationship. And the SCLC mechanism can be expressed as

$$J = \frac{9}{8}\varepsilon_r\varepsilon_0\mu\frac{V^2}{L^3} = \frac{9}{8}\varepsilon_r\varepsilon_0\mu\frac{E^2}{L}, \quad (2)$$

where ε_r is the low frequency dielectric constant, μ is the carrier mobility, and L is the thickness of the thin film.

Under positive bias, leakage currents of all samples follow Ohmic conductive mechanism when the voltage is low.

At some transition points, leakage currents increase sharply, and the voltages of these transition points, as shown in Figure 8, are 2.32 V, 2.75 V, 4.06 V, 5.16 V, and 7.34 V for the samples with the immersing time of 5 min, 30 min, 1 h, 2 h, and 4 h, respectively. In other words, the voltages at the transition point increase with the oxidation time of nickel substrates.

Two factors may account for the phenomenon that the longer the immersing time, the higher the voltage at the transition point. On one aspect, as mentioned above, the decomposition of nickel oxide layer would compensate the oxygen vacancies and thus reduce internal defects in the BTO layer. Since the oxygen vacancies are believed to be related to the origin of the space charges in many ferroelectric materials [32–35], the reduction of oxygen vacancies would increase the transition voltage from the Ohmic conductive mechanism to SCLC conductive mechanism. The second reason may lie in the voltage across the interfacial layer. Due to the compensation of the oxygen vacancies from the interfacial NiO_x layer, the distribution of oxygen vacancies in the BTO layer is not uniform. The area close to the BTO/Ni interface which has deprived oxygen from NiO_x buffer would have a higher resistance and the voltage across this area should be higher. The thicker the original NiO_x buffer is, the thicker the area in the BTO layer which can get enough compensation of oxygen vacancies is, and the higher the voltages would be applied on this area. Moreover, when the original NiO_x layer is thick enough, a residual NiO_x layer would be at the interface after the heat treatment, which would also share more voltage when its thickness increases. The higher partial voltage across the residual NiO_x layer and the interfacial BTO area would result in the increase of the voltage at the transition point.

It is interesting to note that, for the sample whose immersing time is 5 min, the slope of the curve at the high voltage part is not consistent with that of other samples. This suggests that the types of defects in this sample may be different from other samples. In the sample with 5 min immersing time, the interdiffusion between Ni and BTO is not well controlled and the oxygen vacancies in the BTO layer are not well compensated. The related defects would dominate the sources of space charge and lead to a typical SCLC conductive mechanism with the slope of $\ln(J)$ versus $\ln(V)$ close to 2. But when the thickness of NiO_x buffer layer increases and the interdiffusion and oxygen vacancies get a better control, other defects formed during the fabrication process would dominate the sources of space charge. Then the defect-related discrete energy levels appear in the forbidden band. The energy level influences carriers transport and conductive mechanism strongly and leads to a higher slope of $\ln(J)$ versus $\ln(V)$ plot.

4. Conclusions

In summary, the barium titanate (BTO) thin films were successfully deposited on polycrystalline Ni substrates by the polymer assisted deposition (PAD) technique using NiO_x as the buffer layers. It is found that the dielectric properties and the leakage current density of the BTO films are strongly affected by the thickness of NiO_x buffer layers which could be controlled by the pretreatment time. Obvious reduction in dielectric loss and leakage current densities has been observed in the samples with longer pretreatment time of Ni substrates. Combining with the analysis of leakage mechanisms in the BTO layers, the observed phenomena have been proposed to be related to the oxygen compensation and the suppression of interdiffusion at the interface.

Conflict of Interests

The authors declare that there is no conflict of interests regarding the publication of this paper.

Acknowledgments

This work is supported by the National Basic Research Program of China (973 Program) under Grant no. 2015CB351905, the National Natural Science Foundation of China (nos. 51372034, 11329402, and 51172036), and Guangdong Innovative Research Team Program (no. 201001D0104713329).

References

[1] Y. Chen, W. Huang, and B. Peng, "Determination of optimal parameters for dual-layer cathode of polymer electrolyte fuel cell using computational intelligence-aided design," *PLoS ONE*, vol. 9, no. 12, Article ID e114223, 2014.

[2] Q. Zhang, B. Peng, D. Li, Y. Yang, and Y. Liu, "The effect of film microtexture and magnetic field on transparency of Fe_3O_4-PDMS nanocomposite films," *IEEE Photonics Technology Letters*, vol. 26, no. 21, pp. 2181–2184, 2014.

[3] M. Gao, Y. Pan, C. D. Zhang et al., "Tunable interfacial properties of epitaxial graphene on metal substrates," *Applied Physics Letters*, vol. 96, no. 5, Article ID 053109, 2010.

[4] B. Zeng, M. Gao, S. Liu, T. Pan, Z. Huang, and Y. Lin, "Thermal chemical vapor deposition of layered aligned carbon-nanotube films separated by graphite layers," *Physica Status Solidi A: Applications and Materials Science*, vol. 210, no. 6, pp. 1128–1132, 2013.

[5] T. X. Nan, H. Z. Zeng, W. Z. Liang et al., "Growth behavior and photoluminescence properties of ZnO nanowires on gold nanoparticle coated Si surfaces," *Journal of Crystal Growth*, vol. 340, no. 1, pp. 83–86, 2012.

[6] F. W. Van Keuls, R. R. Romanofsky, D. Y. Bohman et al., "$(YBa_2Cu_3O_{7-\delta}$,Au)/$SrTiO_3$/$LaAlO_3$ thin film conductor/ferroelectric coupled microstripline phase shifters for phased array applications," *Applied Physics Letters*, vol. 71, no. 21, pp. 3075–3077, 1997.

[7] D. L. Polla and L. F. Francis, "Processing and characterization of piezoelectric materials and integration into microelectromechanical systems," *Annual Review of Materials Science*, vol. 28, no. 1, pp. 563–597, 1998.

[8] P. Muralt, "Ferroelectric thin films for micro-sensors and actuators: a review," *Journal of Micromechanics and Microengineering*, vol. 10, no. 2, pp. 136–146, 2000.

[9] B. Lin, *Power and energy transduction in piezoelectric wafer active sensors for structural health monitoring: modeling and application [Ph.D. thesis]*, University of South Carolina, Columbia, SC, USA, 2010.

[10] S. M. Aygün, P. Daniels, W. Borland, and J.-P. Maria, "Hot sputtering of barium strontium titanate on nickel foils," *Journal of Applied Physics*, vol. 103, no. 8, Article ID 084123, 2008.

[11] S. Kim, S. Hishita, Y. M. Kang, and S. Baik, "Structural characterization of epitaxial $BaTiO_3$ thin films grown by sputter-deposition on MgO(100)," *Journal of Applied Physics*, vol. 78, no. 9, pp. 5604–5608, 1995.

[12] M. J. Burch, J. Li, D. T. Harris, J.-P. Maria, and E. C. Dickey, "Mechanisms for microstructure enhancement in flux-assisted growth of barium titanate on sapphire," *Journal of Materials Research*, vol. 29, no. 7, pp. 843–848, 2014.

[13] C. L. Jia, K. Urban, S. Hoffmann, and R. Waser, "Microstructure of columnar-grained $SrTiO_3$ and $BaTiO_3$ thin films prepared by chemical solution deposition," *Journal of Materials Research*, vol. 13, no. 8, pp. 2206–2217, 1998.

[14] Z. Yuan, J. Liu, J. Weaver et al., "Ferroelectric $BaTiO_3$ thin films on Ni metal tapes using NiO as buffer layer," *Applied Physics Letters*, vol. 90, no. 20, Article ID 202901, 3 pages, 2007.

[15] J. T. Dawley and P. G. Clem, "Dielectric properties of random and [100] oriented $SrTiO_3$ and $(Ba,Sr)TiO_3$ thin films fabricated on [100] nickel tapes," *Applied Physics Letters*, vol. 81, no. 16, pp. 3028–3030, 2002.

[16] T. Dechakupt, G. Y. Yang, C. A. Randall, S. Trolier-McKinstry, and I. M. Reaney, "Chemical solution-deposited $BaTiO_3$ thin films on Ni foils: microstructure and interfaces," *Journal of the American Ceramic Society*, vol. 91, no. 6, pp. 1845–1850, 2008.

[17] J. Shin, A. Goyal, S. Jesse, and D. H. Kim, "Single-crystal-like, c-axis oriented $BaTiO_3$ thin films with high-performance on flexible metal templates for ferroelectric applications," *Applied Physics Letters*, vol. 94, no. 25, Article ID 252903, 2009.

[18] Q. X. Jia, T. M. McCleskey, A. K. Burrell et al., "Polymer-assisted deposition of metal-oxide films," *Nature Materials*, vol. 3, no. 8, pp. 529–532, 2004.

[19] Y. Lin, J.-S. Lee, H. Wang et al., "Structural and dielectric properties of epitaxial $Ba_{1-x}Sr_xTiO_3$ films grown on $LaAlO_3$ substrates by polymer-assisted deposition," *Applied Physics Letters*, vol. 85, no. 21, pp. 5007–5009, 2004.

[20] Y. Lin, H. Wang, M. E. Hawley et al., "Epitaxial growth of Eu_2O_3 thin tilms on $LaAlO_3$ substrates by polymer-assisted deposition," *Applied Physics Letters*, vol. 85, no. 16, pp. 3426–3428, 2004.

[21] G. F. Zou, J. Zhao, H. M. Luo, T. M. McCleskey, A. K. Burrell, and Q. X. Jia, "Polymer-assisted-deposition: a chemical solution route for a wide range of materials," *Chemical Society Reviews*, vol. 42, no. 2, pp. 439–449, 2013.

[22] W.-Z. Liang, Y.-D. Ji, T.-X. Nan et al., "Optimized growth and dielectric properties of barium titanate thin films on polycrystalline Ni foils," *Chinese Physics B*, vol. 21, no. 6, Article ID 067701, 6 pages, 2012.

[23] W. Liang, Y. Ji, T. Nan et al., "Growth dynamics of barium titanate thin films on polycrystalline Ni foils using polymer-assisted deposition technique," *ACS Applied Materials and Interfaces*, vol. 4, no. 4, pp. 2199–2203, 2012.

[24] W. Liang, Z. Li, Z. Bi et al., "Role of the interface on the magnetoelectric properties of $BaTiO_3$ thin films deposited on polycrystalline Ni foils," *Journal of Materials Chemistry C*, vol. 2, no. 4, pp. 708–714, 2014.

[25] I. Barin, *Thermochemical Data of Pure Substances*, VCH, Weinheim, Germany, 1989.

[26] C. Park, D. P. Norton, D. T. Verebelyi et al., "Nucleation of epitaxial yttria-stabilized zirconia on biaxially textured (001) Ni for deposited conductors," *Applied Physics Letters*, vol. 76, no. 17, pp. 2427–2429, 2000.

[27] J. Chen, P. A. Parilla, R. N. Bhattacharya, and Z. Ren, "Growth of biaxially textured CeO_2/YSZ/CeO_2 and $SrTiO_3$ buffer layers on textured Ni substrates by pulsed laser deposition," *Japanese Journal of Applied Physics*, vol. 43, no. 9, pp. 6040–6043, 2004.

[28] G. W. Dietz, M. Schumacher, R. Waser, S. K. Streiffer, C. Basceri, and A. I. Kingon, "Leakage currents in $Ba_{0.7}Sr_{0.3}TiO_3$ thin films for ultrahigh-density dynamic random access memories," *Journal of Applied Physics*, vol. 82, no. 5, pp. 2359–2364, 1997.

[29] C. S. Hwang, B. T. Lee, C. S. Kang et al., "Depletion layer thickness and Schottky type carrier injection at the interface between Pt electrodes and $(Ba,Sr)TiO_3$ thin films," *Journal of Applied Physics*, vol. 85, no. 1, pp. 287–295, 1999.

[30] A. K. Burrell, T. Mark McCleskey, and Q. X. Jia, "Polymer assisted deposition," *Chemical Communications*, no. 11, pp. 1271–1277, 2008.

[31] C.-J. Peng and S. B. Krupanidhi, "Structures and electrical properties of barium strontium titanate thin films grown by multi-ion-beam reactive sputtering technique," *Journal of Materials Research*, vol. 10, no. 3, pp. 708–726, 1995.

[32] J.-S. Lee, Y. Li, Y. Lin, S. Y. Lee, and Q. X. Jia, "Hydrogen-induced degradation in epitaxial and polycrystalline $(Ba,Sr)TiO_3$ thin films," *Applied Physics Letters*, vol. 84, no. 19, pp. 3825–3827, 2004.

[33] F. M. Pontes, E. R. Leite, E. Longo, J. A. Varela, E. B. Araujo, and J. A. Eiras, "Effects of the postannealing atmosphere on the dielectric properties of $(Ba,Sr)TiO_3$ capacitors: evidence of an interfacial space charge layer," *Applied Physics Letters*, vol. 76, no. 17, pp. 2433–2435, 2000.

[34] K. T. Li and V. C. Lo, "Simulation of oxygen vacancy induced phenomena in ferroelectric thin films," *Journal of Applied Physics*, vol. 97, no. 3, Article ID 034107, 2005.

[35] X. D. Qi, J. Dho, R. Tomov, M. G. Blamire, and J. L. MacManus-Driscoll, "Greatly reduced leakage current and conduction mechanism in aliovalent-ion-doped $BiFeO_3$," *Applied Physics Letters*, vol. 86, no. 6, Article ID 062903, 3 pages, 2005.